Journal of Power Sources 185 (2008) 331–337

Contents lists available at ScienceDirect

Journal of Power Sources

journal homepage: www.elsevier.com/locate/jpowsour

# $Co/LaCrO_3$ composite coatings for AISI 430 stainless steel solid oxide fuel cell interconnects

Nima Shaigan*, Douglas G. Ivey, Weixing Chen

*Department of Chemical and Materials Engineering, University of Alberta, Edmonton, Alberta, Canada T6G 2G6*

ARTICLE INFO

*Article history:*
Received 27 May 2008
Received in revised form 23 June 2008
Accepted 25 June 2008
Available online 5 July 2008

*Keywords:*
Solid oxide fuel cell
Ferritic stainless steel interconnect
Spinel
Composite electrodeposition
Lanthanum chromite
Cobalt

ABSTRACT

Rapidly decreasing electronic conductivity, chromium volatility and poisoning of the cathode material are the major problems associated with inevitable growth of chromia on ferritic stainless steel interconnects of solid oxide fuel cells (SOFC). This work evaluates the performance of a novel, electrodeposited composite $Co/LaCrO_3$ coating for AISI 430 stainless steel. The oxidation behaviour of the $Co/LaCrO_3$-coated AISI 430 substrates is studied in terms of scale microstructure and growth kinetics. Area-specific resistance (ASR) of the coated substrates has also been tested. The results showed that the $Co/LaCrO_3$ coating forms a triple-layer scale consisting of a chromia-rich subscale, a Co–Fe spinel mid-layer and a $Co_3O_4$ spinel top layer at 800 °C in air. This scale is protective, acts as an effective barrier against chromium migration into the outer oxide layer and exhibits a low, stable ASR of ~0.02 Ω cm$^2$ after 900 h at 800 °C in air.



## 1. Introduction

Various grades of ferritic stainless steel (e.g., AISI 430, 434, Crofer 22 APU, Hitachi ZMG 232, etc.) have been used as solid oxide fuel cell (SOFC) interconnects. The marked advantages of the application of ferritic stainless steel for SOFC interconnects include excellent coefficient of thermal expansion (CTE) match with ceramic SOFC components, excellent electrical and thermal conductivity, low cost and ease of fabrication [1–3]. The relatively high-operating temperatures of SOFCs (i.e., 650–800 °C [3]) and the presence of oxygen and fuel, however, result in oxidation of stainless steel interconnects. Stainless steels are chromia-forming alloys. The scale that forms during high-temperature oxidation usually consists of two layers, a chromia subscale and a Mn–Cr spinel outer layer [3]. The formation of a chromia subscale causes serious problems leading to premature degradation of the SOFC stack. Chromium evaporation, poisoning of the cathode material (e.g., lanthanum strontium magnetite) [4,5] and a rapid decrease in electronic conductivity are the well-known critical problems associated with unpreventable formation of chromia scale [1,6]. Moreover, the thermally grown oxide scale forming on most untreated stainless steel interconnects has poor adhesion and is susceptible to cracking and spallation if the SOFC experiences thermal cycles [7].

Recent research studies have focused on developing protective/conductive coatings for steel interconnects to alleviate the aforementioned problems. Among various coatings and surface modifications developed and studied, spinel coatings, in particular, have been attracting considerable attention. Most spinels are acceptably conductive and have matching CTE with other SOFC components [8,9]. Also, spinel coatings are considered as effective barriers against chromium migration and evaporation [10–16]. Although spinel coatings can be applied to the surface of stainless steels utilizing a variety of techniques, electroplating of the transition metals followed by oxidizing in air is the preferred method due to formation of dense, adherent thermally grown spinel layers [9].

In the authors' previous work, the oxidation behavior and electronic conductivity of an electrodeposited composite coating of $LaCrO_3$ particles in a Ni matrix have been studied [17,18]. A double-layer scale consisting of a particle filled chromia-rich subscale and an outer layer composed a Ni–Fe mixed spinel (containing Mn and Cr), together with NiO, forms as the result of oxidation in air at 800 °C. The addition of reactive element containing oxide particles, $LaCrO_3$, greatly improves the oxidation resistance of coated, oxidized AISI 430 steels. Excellent electronic conductivity (ASR ≈ 0.005 Ω cm$^2$ after 400 h of oxidation), good adhesion of the scale and elimination of scale buckling were achieved with this coating system. It has been reported in the literature that Co containing spinels are more conductive than their Ni containing counterparts [8,9]. Therefore, in order to further improve the

* Corresponding author. Tel.: +1 7804928849.
*E-mail address:* nshaigan@ualberta.ca (N. Shaigan).

0378-7753/$ – see front matter © 2008 Elsevier B.V. All rights reserved.
doi:10.1016/j.jpowsour.2008.06.065

**Table 1**
Composition and operating conditions for $Co/LaCrO_3$ composite electroplating

| | |
|---|---|
| Cobalt sulfate, heptahydrate ($CoSO_4 \cdot 7H_2O$) | 450 g $L^{-1}$ (1.6 M) |
| Boric acid ($H_3BO_4$) | 40 g $L^{-1}$ (0.6 M) |
| Sodium dodecyl sulfate (SDS) ($NaC_{12}H_{25}SO_4$) | 0.1 g $L^{-1}$ (0.3 M) |
| Lanthanum chromite ($LaCrO_3$) | 35 g $L^{-1}$ (average particle size is ~1 μm) |
| Temperature | 40 ± 2 °C |
| pH | ~4 (adjusted with NaOH and/or $H_2SO_4$) |
| Agitation | Magnetic bar from the bottom (600 rpm) |
| Current density | 45 mA $cm^{-2}$, DC |
| Anode | Commercially pure Co rod |
| Time (thickness) | 7 min (4–5 μm) |

electronic conductivity, Ni has been replaced with Co in the current work. The present work emphasizes evaluation of the oxidation behavior and electrical properties of electrodeposited composite $Co/LaCrO_3$ coatings applied to AISI 430 ferritic stainless steel substrates.

## 2. Experimental methods

Coupons of AISI 430 stainless steel (measuring 20 mm × 10 mm × 1 mm) were coated with a composite layer of $LaCrO_3$ particles in a Co matrix. The coatings were applied via electroplating in an all-sulfate cobalt plating bath; the composition and operating conditions are shown in Table 1. The plating bath contained 35 g $L^{-1}$ suspended $LaCrO_3$ particles of ~1 μm average size. The cathode and anode were placed horizontally in the plating beaker with the cathode substrate surface facing up. Prior to coating with the composite layer, the specimens were anodically activated to remove the passive film on stainless steels and coated with a thin layer of cobalt (strike plating). The solution composition and conditions for activation/Co strike plating are listed in Table 2. Specimens were ultrasonically cleaned in an alkaline solution prior to activation and after electrodeposition.

Oxidation tests were performed for coated samples in static air at 800 °C for various time periods and up to 2040 h.

The scanning electron microscope (SEM) used for the purpose of imaging and chemical microanalysis was a Hitachi H2700 SEM equipped with a Princeton Gamma-Tech (Prism IG) ultra thin window (UTW) energy dispersive X-ray (EDX) spectrometer. Particle volume fraction of the coatings was determined by means of image analysis software, Image-Pro® Version 6. Phase identification for coated, oxidized specimens was performed by glancing angle X-ray diffraction employing a Rigaku Geigerflex 2173 rotating anode instrument. The incident beam angle was $\theta = 5^\circ$ and the approximate penetration depth was 15 μm. Depth profiling for oxidized $Co/LaCrO_3$-coated specimens was performed by means of secondary ion mass spectrometry (SIMS). An Ion-ToF SIMS IV instrument was employed for this purpose. Specimens were sputtered with $Cs^+$ ions at 1 keV and 250 nA. The sputtering area was 200 μm × 200 μm. $Ga^+$ ion sputtering at 15 keV over an area of 34 μm × 34 μm was used for analysis. A Sartorius (CP225D) high-precision balance was used to measure sample weight gain after oxidation. For this purpose, three identical samples were used and the results were averaged.

**Table 2**
Composition and operating conditions of activation/Co strike plating

| | |
|---|---|
| Cobalt chloride, hexahydrate ($CoCl_2 \cdot 6H_2O$) | 100 g $L^{-1}$ (0.42 M) |
| Hydrochloric acid (HCl, 37 vol%) | 85 mL $L^{-1}$ (1 M) |
| Anodic activation | 2 min, 22 mA $cm^{-2}$ |
| Cathodic cobalt strike | 6 min, 22 mA $cm^{-2}$ |
| Temperature | 20 °C |
| Anode | Commercially pure Co rod |

The design schematically shown in Fig. 1 was used to measure the area-specific resistance (ASR) of the oxidized $Co/LaCrO_3$-coated and -uncoated specimens. This test method is similar to that used and described in authors' previous work [18]. Pre-oxidation of Pt wire welded samples was performed at 800 °C in air for ~24 h in order to avoid alloy-to-alloy adhesion. Instead of conductive paste, a static load of 9.8 N was applied to the samples to ensure a reliable electrical contact between the samples. A constant current density of 200 mA $cm^{-2}$ was applied and the voltage was recorded by a Gamry computer, Series G 300, every 300 s. The resistance and ASR, which is the product of resistance and apparent surface area, were calculated according to Ohm's law. In order to measure the resistance contribution from the junctions, wires and the alloy, two platinum wires were spot welded to the sides of a single AISI 430 coupon and the resulting resistance was subtracted from the original test results. This results in the pure resistance from the scales. All the above-mentioned tests were run at 800 °C in an electrical box furnace and static air.

## 3. Results and discussion

### 3.1. As-deposited composite $Co/LaCrO_3$ coating

Fig. 2(a) and (b) illustrate the as-deposited coating surface and cross-sectional structure. Uniform embedding of $LaCrO_3$ particles in the Co matrix is seen. The coating has a uniform thickness and exhibits good adhesion to the substrate. These samples were prepared according to the conditions described in Table 1. Image analysis from the plan view image (Fig. 2(a)) shows ~20 vol% of embedded particles in the coating.

### 3.2. Oxide scale structure and morphology

Surface and cross-sectional SEM images of $Co/LaCrO_3$-coated AISI 430 stainless steel coupons oxidized for 170 and 2040 h at 800 °C are illustrated in Fig. 3. A nodular surface morphology with uniform-size oxide particles is observed on the surface of both oxidized specimens (Fig. 3(a) and (c)). Some porosity is seen on the oxide surfaces. The cross-sectional backscattered electron (BSE) images (Fig. 3(b) and (d)) show three different layers in the scale. Some porosity is also present at the scale–metal interface for the sample oxidized for 2040 h (Fig. 3(d)). The EDX results from the numbered regions in Fig. 3(b) and (d) are listed in Table 3. Glancing angle X-ray diffraction patterns were also obtained to identify the phases in the oxide scales for the samples oxidized for 170 and 2040 h. The XRD patterns are shown in Fig. 4. The three layers of the scale have been identified to be FCC-spinel $Co_3O_4$ (JCPDS file: 65-3103 [19]), containing Fe and a small amount of Cr, as the outer layer, $(Co, Fe)_3O_4$ FCC-spinel (closely matching $CoFe_2O_4$, JCPDS file: 03-0864 [19]), containing small amounts of Cr and Mn, as the mid-layer, and a $LaCrO_3$ (JCPDS file: 33-0701 [19]) particle filled chromia-rich (JCPDS file: 38-1479 [19]) layer, also containing Co, Fe and Mn, as the inner layer. The peaks corresponding to the chromia-rich phase are not very intense for the sample oxidized for 2040 h. This is due to the increased thickness of the scale which limits penetration and/or diffraction of the incident X-rays. The thickness of chromia-rich scale after 2040 h of oxidation is ~2 μm.

Formation of porosity at the interface of the outer $Co_3O_4$ and mid-Co–Fe spinel layers, as well as on the surface of scale, is attributed to the unusually large CTE of $Co_3O_4$ spinel at high temperatures (>600 K). The CTE of undoped $Co_3O_4$ is reported to be

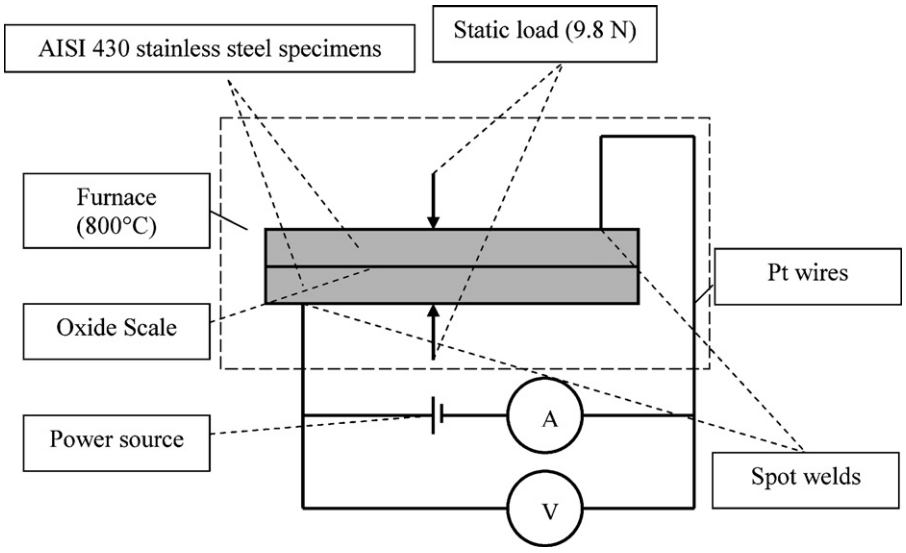


**Fig. 1.** Experimental setup for measuring the electrical contact resistance of oxide scales.

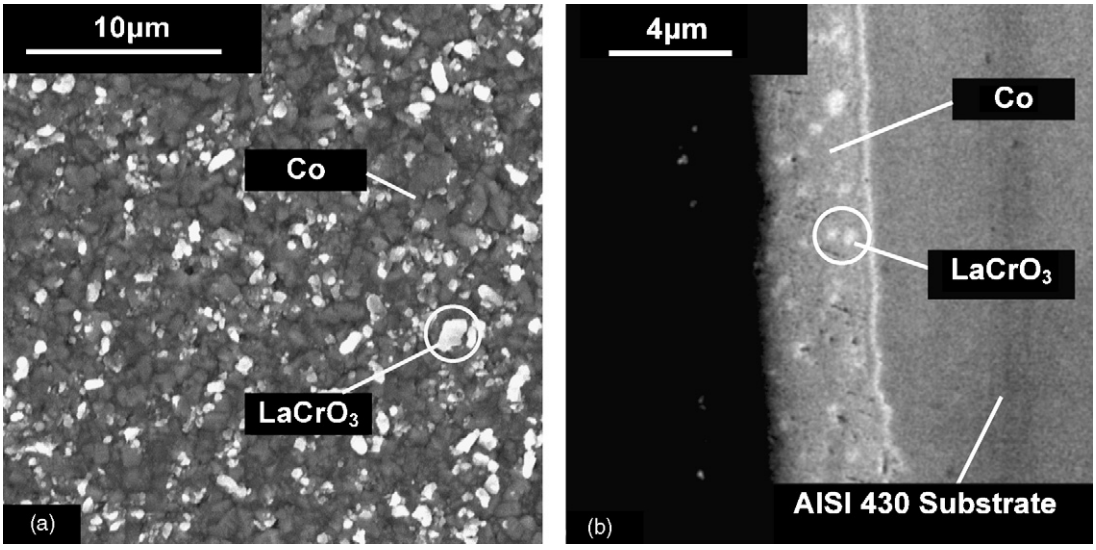


**Fig. 2.** SEM images of the as-deposited Co/$LaCrO_3$ coating: (a) surface secondary electron (SE); (b) cross-sectional backscattered electron (BSE) image.

$\sim 40 \times 10^{-6}$ ($K^{-1}$) [20,21] at 800 °C, which is approximately four times larger than similar values for most Co containing spinels ($\alpha \approx 7–14 \times 10^{-6}$ ($K^{-1}$) [8,9,20]). According to Broemme [20], the anomalously large CTE of $Co_3O_4$ at temperatures higher than 750 K is due to inter-atomic transition of non-magnetic $Co^{3+}$ ions on octahedral sites into a magnetic state with a larger ionic radius. This results in expansion of the spinel lattice. The large CTE for the $Co_3O_4$ layer results in a considerable amount of shrinkage in the layer compared with the underlying $(Co, Fe)_3O_4$ layer during cooling of the sample from 800 °C, which is the temperature at which a stress-free oxide scale forms. This shrinkage results in detachment of oxide particles in the $Co_3O_4$ layer and at the $Co_3O_4$/$(Co, Fe)_3O_4$ interface.

### 3.3. SIMS depth profiles

The distribution of metallic elements throughout the scale was analyzed by means of SIMS depth profiling. Depth profiles

**Table 3**
Chemical composition (at%) and phases for the numbered regions in Fig. 3(b) and (d) as determined by EDX/XRD analysis

| Regions (points) | Phase | 170 h (Fig. 3(b)) | | | | 2040 h (Fig. 3(d)) | | | |
|---|---|---|---|---|---|---|---|---|---|
| | | Fe | Co | Cr | Mn | Fe | Co | Cr | Mn |
| (1) | $Co_3O_4$ spinel | 8 | 81 | 1 | 0 | 3 | 87 | 0.5 | 0 |
| (2) | $(Co, Fe)_3O_4$ spinel | 43 | 41 | 2 | 1 | 32 | 54 | 2 | 1 |
| (3) | Chromia-rich | 24 | 15 | 43 | 1 | 3 | 21 | 58 | 2 |
| (4) | α-Fe–Cr–Co | 63 | 24 | 11 | 1 | 83 | 1 | 14 | 1 |

Oxygen levels are not shown.

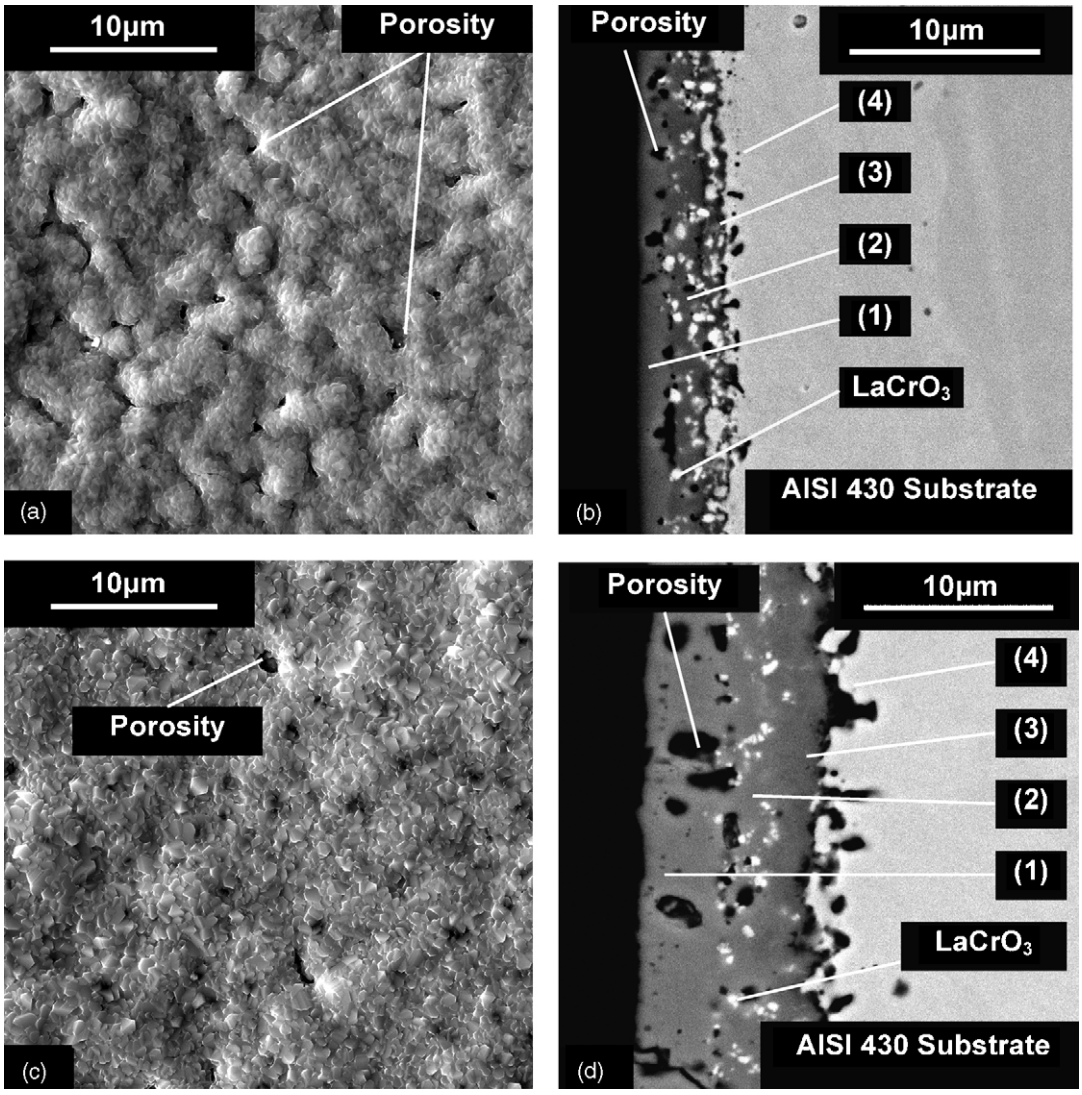


**Fig. 3.** SEM images of oxidized Co/$LaCrO_3$ coatings: (a and b) after 170 h; (c and d) after 2040 h of oxidation in air at 800 °C. (a) and (c) are surface SE images; (b) and (d) are cross-sectional BSE images.

for Co/$LaCrO_3$-coated specimens oxidized for 170 and 2040 h are shown in Fig. 5(a) and (b), respectively. Intensity profiles for Cr show a maximum in the inner scale for both samples. The Cr intensity in the outer scale is small even for the sample oxidized for 2040 h. The Cr intensity increase at the outside surface is due to a faster ionization rate of Cr from the scale surface during depth profiling and is an artefact. This indicates that Cr migration to the scale surface has been effectively reduced. The intensity profiles for Fe and Co exhibit a similar increase in the mid-spinel layer where Mn also exhibits an increase. The major element contributing to the outer scale is Co. Small amounts of Fe and Cr are also present in the outer layer as they were detected by EDX (regions (1) in Table 3). Diffusion of Mn through the inner layer into the mid-layer is seen in Fig. 5(a) and (b). Lanthanum exists in the entire oxide scale with a very small concentration in the outer $Co_3O_4$ layer. Segregation of Si (likely as $SiO_2$) underneath the chromia-rich inner scale is apparent, particularly in Fig. 5(b). The porosity at the scale–metal interface (Fig. 3(d)) may have formed due to the formation of a silica network. Silica is not miscible with chromia, and the poor adhesion between the oxides may cause detachment of chromia from silica, which is adherent to the substrate, during the development of thermal stresses. Stainless steel substrates with lower Si levels may be more promising.

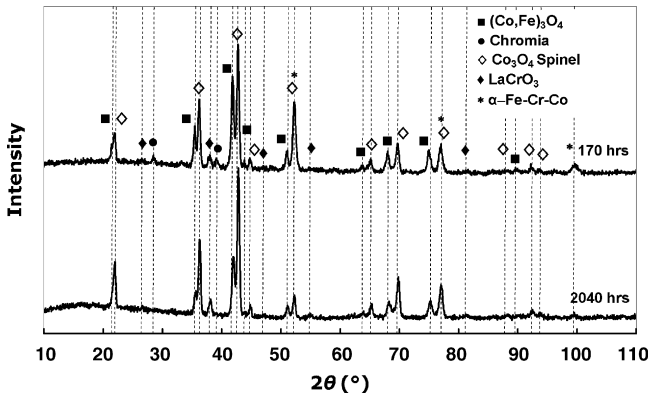


**Fig. 4.** XRD patterns for Co/$LaCrO_3$-coated specimens oxidized for 170 and 2040 h.

### 3.4. *Effect of $LaCrO_3$ particles*

In order to investigate the effect of $LaCrO_3$ particle addition on the oxidation behavior of coated steels, substrates of AISI 430 steel

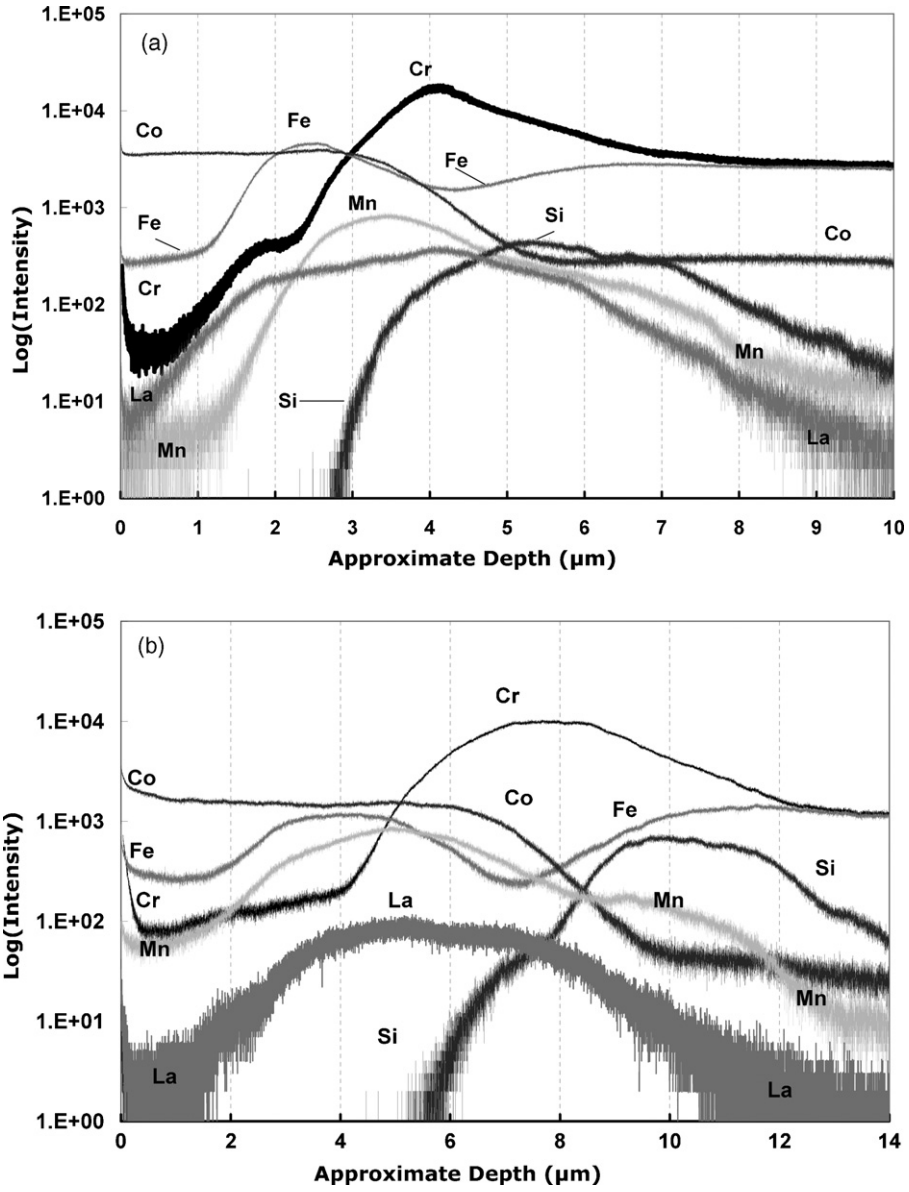


**Fig. 5.** SIMS depth profiles for oxidized Co/$LaCrO_3$-coated specimens for (a) 170 h and (b) 2040 h of oxidation.

were coated with pure Co to the same thickness as the composite Co/$LaCrO_3$ coatings (~4–5 μm) and oxidized under identical conditions. For these samples, however, the scale partially spalled off after ~1200 h of oxidation. Fig. 6 illustrates the specific weight gains as a function of time for oxidized uncoated, Co-coated and Co/$LaCrO_3$-coated steel coupons. For the coated samples, the initial oxidation rate is considerably higher than that for uncoated samples. This is due to rapid oxidation of Co in the coatings. After ~100 h of oxidation, however, the Co/$LaCrO_3$-coated samples show similar oxidation kinetics to the uncoated steels. The Co-coated specimens exhibit a higher oxidation rate in comparison with the Co/$LaCrO_3$-coated coupons.

Fig. 7(a) and (b) show surface and cross-sectional SEM images of Co-coated samples oxidized for 170 h. The scale structure is similar to that which grows on Co/$LaCrO_3$-coated samples, except that in this case the scale is thicker and no particles are present. The scale is composed of three visible layers which are numbered on the images. Table 4 shows the composition and phases present in

**Table 4**
Chemical composition (at%) and phases for the numbered regions in Fig. 7(b) and (d) as determined by EDX/XRD analysis

| Regions (points) | Phase structure | 170 h (Fig. 7(b)) | | | | 1200 h (Fig. 7(d)) | | | |
|---|---|---|---|---|---|---|---|---|---|
| | | Fe | Co | Cr | Mn | Fe | Co | Cr | Mn |
| (1) | $Co_3O_4$ spinel | 8 | 81 | 1 | 1 | 9 | 80 | 1 | 1 |
| (2) | $(Co, Fe)_3O_4$ spinel | 42 | 38 | 5 | 1 | 10 | 76 | 1 | 1 |
| (3) | Chromia-rich | 5 | 2 | 77 | 1 | 4 | 3 | 74 | 2 |
| (4) | α-Fe–Cr–Co | 80 | 12 | 12 | 1 | 77 | 7 | 11 | 1 |

Oxygen levels are not shown.

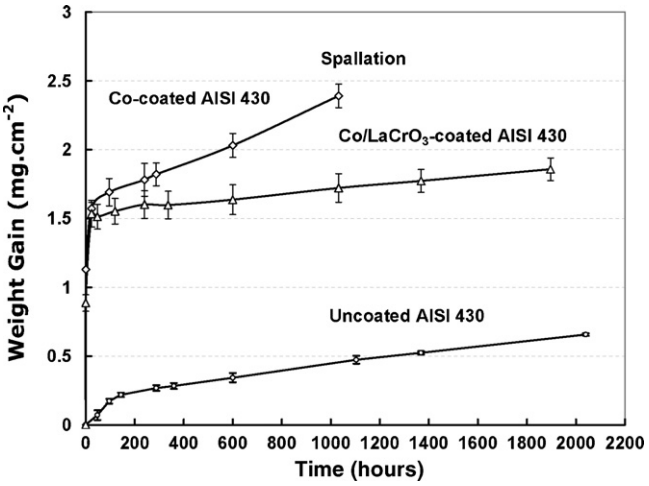


**Fig. 6.** Specific weight gains for oxidized $Co/LaCrO_3$-coated, Co-coated and -uncoated AISI 430 coupons as a function of oxidation time.

the scale, determined by EDX and XRD analysis. The three layers in the scale are a chromia-rich inner layer, a mixed Co–Fe–Cr spinel mid-layer and a $Co_3O_4$ outer layer. Fig. 7(c) and d depict the oxide scale after 1200 h of oxidation. The cross-sectional image (Fig. 7(d)) shows a thick scale consisting of a thick, non-adherent chromia-rich layer covered by two porous outer layers. The composition and structure of the layers are also listed in Table 4. Fig. 7(c) shows a spalled area of the scale; underneath the scale are isolated, dark islands of silica, as determined by EDX analysis. Since silica is not entirely removed by the spalled scale (Fig. 7(c)), there is inadequate adhesion between chromia and silica (silica is not miscible with chromia). This poor adhesion and formation of a silica network at the alloy-scale interface may be a reason for spallation of the scale.

For uncoated AISI 430, the oxide scale consists of a chromia-rich subscale covered by a Mn–Cr spinel layer. A thin layer of silica also forms beneath the chromia-rich layer. After 170 h of oxidation at 800 °C in air, the scale is ~1 μm thick and grows to a thickness of ~2 μm after 2040 h of oxidation.

The addition of $LaCrO_3$ particles to the coating not only decreases the oxidation rate but also eliminates scale spallation. The mechanisms through which $LaCrO_3$ particles enhance the oxidation properties of the coating are not clear for this case. A similar

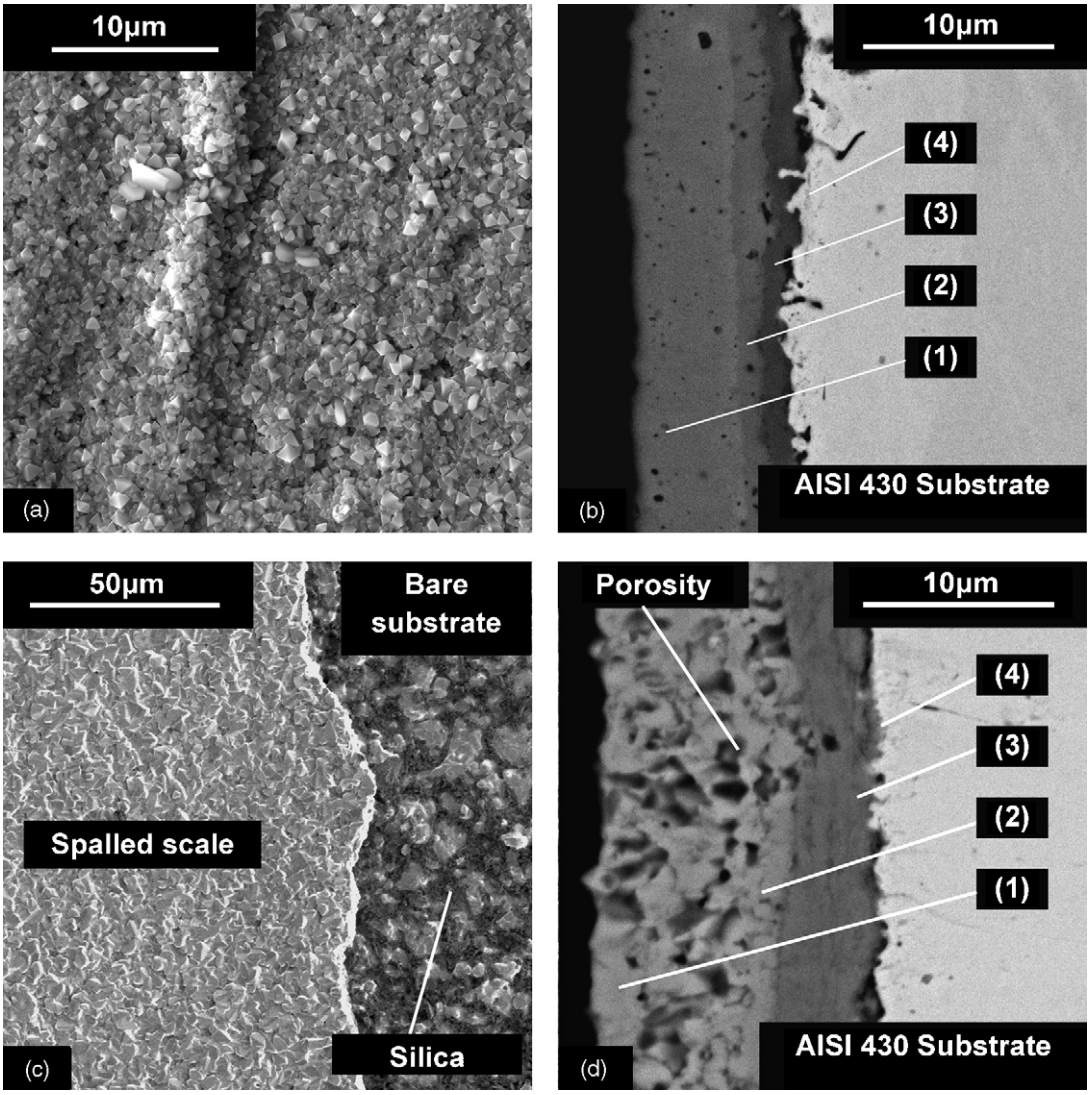


**Fig. 7.** SEM images of oxidized Co coatings: (a and b) after 170 h; (c and d) after 1200 h of oxidation in air at 800 °C. (a) and (c) are surface SE images; (b) and (d) are cross-sectional BSE images.

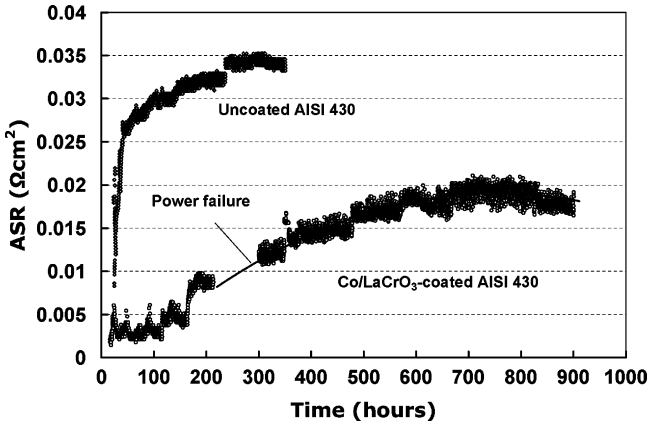


**Fig. 8.** ASR values for $Co/LaCrO_3$-coated and -uncoated AISI 430 stainless steel at 800 °C in air as a function of time.

effect has been observed for $Ni/LaCrO_3$ coatings developed for stainless steel interconnects and studied in the authors' previous work [17,18]. The beneficial effects and mechanisms of oxidation resistance improvement of reactive elements have been reviewed by Whittle and Stringer [22].

### 3.5. Area-specific resistance

The ASR for $Co/LaCrO_3$-coated and -uncoated AISI 430 stainless steels, as a function of time, are plotted in Fig. 8. ASR values for uncoated AISI 430 increase rapidly with oxidation time for up to ~50 h and approach a constant value of 0.035 Ω cm$^2$ after ~250 h with a parabolic trend. $Co/LaCrO_3$-coated specimens, however, show a very low resistance (ASR < 0.005 Ω cm$^2$) for up to ~165 h of oxidation. The ASR starts to increase parabolically after this point and approaches a constant value of ~0.02 Ω cm$^2$ after ~600 h of oxidation. No further increase in ASR for $Co/LaCrO_3$-coated steels is seen for the test time of 900 h. The sudden increase in ASR after 160 h is attributed to formation of porosity at the metal–scale interface which reduces the actual area of contact between the scale and substrate. This porosity, which is visible in Fig. 3(d), may be due to outward diffusion of Co. SIMS results (Fig. 5) show the outward diffusion of Co through the chromia-rich inner layer. The increase in the thickness of the outer layer, which is Co-rich, also suggests that there is outward diffusion of Co through the chromia-rich inner layer. Therefore, the chromia-rich subscale is not protective enough against the outward diffusion of Co.

Several factors can contribute to the improved electronic conductivity for the $Co/LaCrO_3$-coated steels over uncoated AISI 430 steels. These include the higher electronic conductivity of the scale consisting of Co containing spinel layers, the presence of conductive perovskite $LaCrO_3$ particles in the oxide scale, improved adhesion of the scale to the substrate and elimination of scale spallation.

## 4. Conclusions

The application of composite $Co/LaCrO_3$ coatings for AISI 430 stainless steel was studied as a potential solution to limit chromium migration and increase high-temperature electronic conductivity of the substrate. The scale, which forms on the surface of oxidized $Co/LaCrO_3$-coated AISI 430 at 800 °C in air, consists of two layers of cobalt containing spinel, a Co–Fe spinel as the mid-layer and $Co_3O_4$ as the top layer, and a chromia-rich inner layer. The mid- and inner layers of the scale contain $LaCrO_3$ particles. The coating limits the diffusion of Cr into the scale surface to less than 1 at% Cr after 2040 h of oxidation. The addition of $LaCrO_3$ particles not only improves the oxidation resistance of the coating but also eliminates scale spallation. The ASR of $Co/LaCrO_3$-coated AISI 430 steels does not exceed ~0.02 Ω cm$^2$ after 900 h at 800 °C in air. Silica networks, which form at the metal–scale interface, result in spallation of scale in Co-coated steels and pore formation in $Co/LaCrO_3$-coated specimens. This may be a problem for long-term service. A low-silicon grade substrate may be more suitable for $Co/LaCrO_3$ coatings.

## Acknowledgements

The authors wish to thank Versa Power Systems, Inc. and the Natural Sciences and Engineering Research Council (NSERC) of Canada for providing research funding.

## References

[1] W.Z. Zhu, S.C. Deevi, Mater. Res. Bull. 38 (2003) 957–972.
[2] W.Z. Zhu, S.C. Deevi, Mater. Sci. Eng. A 348 (2003) 227–243.
[3] Z. Yang, Int. Mater. Rev. 53 (2008) 39–54.
[4] S.P. Jiang, J.P. Zhang, L. Apateanu, K. Foger, J. Electrochem. Soc. 147 (11) (2000) 4013–4022.
[5] Y. Matsuzaki, I. Yasuda, Solid State Ionics 132 (2000) 271–278.
[6] S. Fontana, R. Amendola, S. Chevalier, P. Piccardo, G. Caboche, M. Viviani, R. Molins, M. Sennour, J. Power Sources 171 (2007) 652–662.
[7] G. Cabouro, G. Caboche, S. Chevalier, P. Piccardo, J. Power Sources 156 (2006) 39–44.
[8] W. Qu, L. Jian, J.M. Hill, D.G. Ivey, J. Power Sources 153 (2006) 114–124.
[9] A. Petric, H. Ling, J. Am. Ceram. Soc. 90 (5) (2007) 1515–1520.
[10] X. Chen, P.Y. Hou, C.P. Jacobson, S.J. Visko, L.C. De Jonghe, Solid State Ionics 176 (2005) 425–433.
[11] Z. Yang, G. Xia, S.P. Simner, J.W. Stevenson, J. Electrochem. Soc. 152 (9) (2005) 1896–1901.
[12] Z. Yang, G. Xia, X. Li, J.W. Stevenson, Int. J. Hydrogen Energy 32 (2007) 3648–3654.
[13] Z. Yang, G. Xia, J.W. Stevenson, Electrochem. Solid-State Lett. 8 (3) (2005) A168–A170.
[14] M.R. Bateni, P. Wei, X. Deng, A. Petric, Surf. Coat. Technol. 201 (2007) 4677–4684.
[15] P. Wei, X. Deng, M.R. Bateni, A. Petric, Corrosion 63 (2007) 529–536.
[16] X. Deng, P. Wei, M.R. Bateni, A. Petric, J. Power Sources 160 (2006) 1225–1229.
[17] N. Shaigan, D.G. Ivey, W. Chen, J. Electrochem. Soc. 155 (4) (2008) D278–D284.
[18] N. Shaigan, D.G. Ivey, W. Chen, J. Power Sources 183 (2008) 651–659.
[19] JCPDS, International Center for Diffraction Data, Newtown Square, PA, 1996.
[20] A.D.D. Broemme, IEEE Trans. Electric. Insul. 26 (1) (1991) 49–52.
[21] V.A.M. Brabers, A.D.D. Broemme, J. Magn. Magn. Mater. 104–107 (1992) 405–406.
[22] D.P. Whittle, J. Stringer, Philos. Trans. R. Soc. Lond. A: Math. Phys. Sci. 295 (1980) 309–329.